

# Assessment of the Energy Efficiency of Ammonia Production by Microbubbles

Ferenc Kubicsek<sup>1</sup>, Ferenc Hegedűs<sup>1\*</sup>

<sup>1</sup> Department of Hydrodynamic Systems, Faculty of Mechanical Engineering, Budapest University of Technology and Economics, P. O. B. 91, H-1521 Budapest, Hungary

\* Corresponding author, e-mail: [fhegedus@hds.bme.hu](mailto:fhegedus@hds.bme.hu)

Received: 30 June 2023, Accepted: 17 November 2023, Published online: 27 May 2024

## Abstract

The present paper investigates the energy efficiency of ammonia production by a freely oscillating microbubble placed in an infinite domain of liquid. The spherical bubble initially contains a mixture of nitrogen and hydrogen. The bubble is expanded from its equilibrium size to a specific maximum radius via an isothermal expansion. The work needed to expand the bubble is its potential energy calculated by the sum of the work done by the internal gas, the work needed to displace the mass of the surrounding liquid, and the work needed to increase the area of the bubble against the surface tension. During the radial pulsation of the freely oscillating bubble, the internal temperature can reach several thousands of degrees of Kelvin inducing chemical reactions. The chemical yield is computed by solving a set of ordinary differential equations describing the radial dynamics of the bubble (Keller—Miksis equations), the temporal evolution of the internal temperature (first law of thermodynamics), and the concentration of the chemical species (reaction mechanism). The control parameters during the simulations were the equilibrium bubble size, initial expansion ratio, ambient pressure, and the initial concentration ratio of nitrogen and hydrogen. In the best-case scenario, the energy requirement in terms of GJ/t is 6.8 times higher than the best available facility of the Haber—Bosch process (assuming that the hydrogen is produced via the electrolysis of water).

## Keywords

ammonia, Haber—Bosch process, bubble dynamics, microbubbles, energy efficiency

## 1 Introduction

Ammonia plays a vital and important role in the globalized economy [1]. As a primary commodity for nitrogen fertilizers, the existence of modern agriculture depends heavily on a reliable source of ammonia. In fact, 70% of the produced ammonia is used as fertilizers. It is the most energy and emission-intensive chemical industry. The global average energy intensity is about 46.2 GJ/t (the best available technology is approximately 28 GJ/t), and the emission intensity is nearly 24 t CO<sub>2</sub>/t. In comparison, the corresponding values for steel and cement production are 19.4 GJ/t, 2.4 GJ/t, and 1.4 t CO<sub>2</sub>/t, 0.6 t CO<sub>2</sub>/t, respectively. The magnitude of the ammonia industry can also be quantified by its natural gas consumption: more than 20% of the unearched methane is used for feedstock (methane steam reforming for hydrogen). Thus, any serious policy that attempts to reach net-zero emission by 2050 needs to address the issue of "Green Ammonia".

Today, ammonia is produced by the more than a hundred-year-old technology called the Haber-Bosch process [2–4]. It requires high temperature (500 °C) and pressure (400 bar), which makes the process and the necessary equipment expensive and dangerous. The hydrogen (obtained from methane or from the electrolysis of water) and the nitrogen (obtained by air separation) are reacted catalytically. The process is difficult. High temperature is needed to increase the reaction rate to an acceptable level. However, the equilibrium for ammonia favors low temperatures. Therefore, to increase the equilibrium concentration of ammonia, high pressure is a requirement.

The present study focuses on an alternative way of producing ammonia from bubbles containing nitrogen and hydrogen. The underlying physical phenomenon is the extreme dynamics of microbubbles observed in the scientific field of cavitation [5, 6]. In a fluid flow system,

such bubbles in a liquid domain, e.g., in water, exhibit expansion in low-pressure regions (for instance, due to high velocity or in the rarefaction phase of ultrasound). The expansion (maximum bubble radius) can be an order of magnitude higher than the equilibrium size of the bubble. If the bubble travels into a high-pressure region, it starts to compress very rapidly, called bubble collapse. Due to the possibly high compression ratio, the temperature inside the bubble can reach several thousands of degrees of Kelvin inducing chemical reactions [7–15]. In this regard, the bubbles can be considered as micron-sized chemical reactors. Because of the large energy-focusing mechanism that occurs during a bubble collapse, the high activation energy of  $N_2$  dissociation, caused by the triple bond of nitrogen molecule, can easily be reached. Moreover, the high compression ratio means extremely high internal pressure (usually in the order of thousands of atmospheres), which is a favorable environment for high ammonia equilibrium concentration.

There are two widely employed ways to generate and/or excite bubbles: hydrodynamic [16] and acoustic cavitation [6]. Although in both techniques, bubbles appear as clusters, which have complex dynamics [17, 18], the present paper focuses on the single spherical bubble that can be considered as a building block of a more complex cavitation reactor. One of the reasons is the reported low energy efficiency of ammonia production by cavitation [19]: approximately 882353 GJ/t, which is several orders of magnitude larger than that of the Haber–Bosch process. In the present study, the authors show that the experiment mentioned was highly suboptimal and that the energy efficiency can be as low as 265 GJ/t. Although this value is still approximately six times higher than the Haber–Bosch process, it is a significant step to make ammonia production by bubbles an energetically viable alternative.

The key aspect of our approach is that the input energy and the chemical yield of a single freely oscillating bubble are connected consistently. More precisely, the energy required to expand a bubble is obtained by calculating its potential energy at the maximum radius (sum of the work done by the internal gas, the work done on the liquid domain, and by expanding the bubble area against the surface tension); and the chemical yield is computed by numerical simulation of the governing equations including chemical kinetics.

It is important to stress that we focus on theoretical energy considerations based on an idealized test case. The technique of the generation of microbubbles, their

spherical stability [20, 21], the effect of mass transfer at the bubble interface (e.g. evaporation/condensation) and the effect of bubble-bubble interactions [22] are out of the scope of the present study. Instead, we focus on optimizing the most important parameters that occur in the single bubble system: initial (equilibrium) bubble size, expansion ratio, ambient pressure, and initial composition. Although the simplifications mentioned above can have a significant influence and should be taken into account in a more detailed investigation in the future, the more than three orders of magnitude increase in energy efficiency (882353 GJ/t vs. 265 GJ/t) is still a valuable result of the present study. After presenting the results, a possible reason for the poor experimental outcome in [19] is also discussed.

## 2 The governing equations

We can separate the mathematical model of a sonochemical bubble into two main parts: physical and chemical models. The physical model describes the radial pulsation of the bubble and the fluctuation of the temperature and pressure inside the bubble, while the chemical model deals with the chemical reactions in the bubble interior.

The equation system involves a large number of constants for the description of the reaction mechanism (taken from [23]) and for the NASA polynomials to compute the material properties. In order to avoid the inclusion of these data as large tables in the main paper, they are provided as an OpenSMOKE++ reaction mechanism file in the Supporting Information.

### 2.1 General description of the reaction mechanism

In general, we can write a chemical reaction in the form



where  $\nu_{ki}$  are the stoichiometric coefficients and  $\chi_k$  is the chemical symbol of the  $k^{\text{th}}$  species. There are  $K$  types of species in the system; that is,  $k = 1, \dots, K$ . The index of the reactions is  $i = 1, \dots, I$ , where  $I$  is the number of the reactions. The upper index  $f$  means forward; the upper index  $b$  means backward reactions. In reaction kinetics, the reaction rates are calculated as

$$q_i = k_{f_i} \cdot \prod_{k=1}^K c_k^{\nu_{ki}^f} - k_{b_i} \cdot \prod_{k=1}^K c_k^{\nu_{ki}^b}, \quad (2)$$

where  $k_{f_i}$  is the  $i^{\text{th}}$  forward,  $k_{b_i}$  is the  $i^{\text{th}}$  backward reaction rate coefficients, and  $c_k$  is the concentration of the  $k^{\text{th}}$  species. The production rate of each species is

$$\dot{\omega}_k = \sum_{i=1}^I v_{ki} \cdot q_i, \quad (3)$$

where  $v_{ki} = v_{ki}^b - v_{ki}^f$ . The  $i^{\text{th}}$  forward rate coefficient is generally calculated from the extended Arrhenius-equation written as

$$k_{f_i} = A_i \cdot T^{b_i} \cdot \exp\left(\frac{-E_i}{R_g \cdot T}\right), \quad (4)$$

where  $A_i$  is the pre-exponential factor,  $b_i$  is the temperature exponent,  $E_i$  is the activation energy, and  $R_g$  is the universal gas constant. The backward rate constants  $k_{b_i}$  are calculated from the equilibrium constants defined as

$$K_{c_i} = \frac{k_{f_i}}{k_{b_i}}. \quad (5)$$

The equilibrium constants have the form of

$$K_{c_i} = K_{p_i} \cdot \left(\frac{P_{atm}}{R_g \cdot T}\right)^{\sum_{k=1}^K v_{ki}}, \quad (6)$$

where  $P_{atm}$  is the atmospheric pressure, and  $K_{p_i}$  is calculated via

$$K_{p_i} = \exp\left(\frac{\Delta S_i}{R_g} - \frac{\Delta H_i}{R_g \cdot T}\right). \quad (7)$$

In Eq. (7),  $\Delta S_i$  and  $\Delta H_i$  are

$$\frac{\Delta S_i}{R_g} = \sum_{k=1}^K v_{ki} \cdot \frac{S_k}{R_g} \quad (8)$$

and

$$\frac{\Delta H_i}{R_g \cdot T} = \sum_{k=1}^K v_{ki} \cdot \frac{H_k}{R_g \cdot T}, \quad (9)$$

respectively. Here,  $S_k$  and  $H_k$  are the molar entropy and molar enthalpy of formation of species  $k$  at temperature  $T$ . The notation  $\Delta$  means the total change in a forward reaction (from reactants to products).

There are other types of reaction rates that cannot be described accurately enough by the Arrhenius equation. The first type is of three-body reactions, which are often dissociation or recombination reactions. This type of reaction needs a third molecule which removes the excess energy of the energetically excited reaction intermediate. Every molecule present can be a third body, but the larger molecules are more effective. We can take the efficiency into account in a third-body collision efficiency factor via the modification of the reaction rates as

$$q'_i = q_i \cdot [M], \quad (10)$$

where

$$[M] = \sum_{k=1}^K \alpha_{ki} \cdot c_k, \quad (11)$$

is the effective total concentration of the third-body species, and  $\alpha_{ki}$  is the matrix of the third-body efficiencies.

Some reaction rate constants are pressure-dependent (besides depending on temperature). First, the high-pressure limit reaction rate coefficient ( $k_\infty$ ) and the low-pressure limit reaction rate coefficient ( $k_0$ ) have to be calculated via Eq. (12) and Eq. (13):

$$k_\infty = A_\infty \cdot T^{b_\infty} \cdot \exp\left(\frac{-E_\infty}{R_g \cdot T}\right), \quad (12)$$

and

$$k_0 = A_0 \cdot T^{b_0} \cdot \exp\left(\frac{-E_0}{R_g \cdot T}\right). \quad (13)$$

Next, the overall rate constant is given by

$$k'_{f_i} = k_\infty \cdot \frac{P_r}{1 + P_r} \cdot F, \quad (14)$$

where the blending function,  $F$  controls the shape of the  $k'_{f_i} - P_r$  curve, the reduced pressure is described as

$$P_r = \frac{k_0}{k_\infty} \cdot [M]. \quad (15)$$

Here,  $[M]$  is the total concentration of the mixture enhanced by the third-body efficiencies, see Eq. (11). In Eq. (15), the effective total concentration  $[M]$  is already applied; consequently, it does not need to be multiplied again while calculating  $q'_i$  in Eq. (10). There are several approaches to calculate  $F$  in Eq. (14). In the Lindemann formalism,  $F = 1$ . In the Troe formalism,  $F$  is computed from the following set of equations:

$$\log_{10} F = \left[ 1 + \left[ \frac{\log_{10} P_r + c}{n - d \cdot (\log_{10} P_r + c)} \right]^2 \right]^{-1} \cdot \log_{10} F_{cent}, \quad (16)$$

where  $F_{cent}$  is the broadening parameter,

$$c = -0.4 - 0.67 \cdot \log_{10} F_{cent}, \quad (17)$$

$$n = 0.75 - 1.27 \cdot \log_{10} F_{cent}, \quad (18)$$

$$d = 0.14, \quad (19)$$

and

$$F_{cent} = (1 - \alpha) \cdot \exp\left(\frac{-T}{T^{***}}\right) + \alpha \cdot \exp\left(\frac{-T}{T^*}\right) + \exp\left(\frac{-T^{**}}{T}\right). \quad (20)$$

Equations (16)–(20) give the following limit cases:

$$k_{fi} \rightarrow \begin{cases} k_{\infty}, & \text{if } p \rightarrow \infty \\ k_0 \cdot [M], & \text{if } p \rightarrow 0. \end{cases} \quad (21)$$

In Eq. (20), the four parameters ( $\alpha$ ,  $T^{***}$ ,  $T^*$ ,  $T^{**}$ ) are the Troe parameters, which can be different for each Troe-form reaction. In some reactions,  $T^{**}$  is not given; in this case, the last term in Eq. (20) is neglected.

The next way of defining the pressure dependence of a reaction rate is based on the PLOG formalism, where the forward reaction rate coefficients depend on the pressure logarithmically. Usually, several pressure levels  $P_j$  are given with an Arrhenius set ( $A_j$ ,  $\beta_j$ ,  $E_j$ ) for each reaction. The forward reaction rate coefficient for the  $j^{\text{th}}$  pressure level is described as

$$k_j = k(T, P_j) = A_j T^{\beta_j} \exp\left(-\frac{E_j}{R_g \cdot T}\right). \quad (22)$$

If the pressure is between  $P_j$  and  $P_{j+1}$ , then the natural logarithm of  $k$  is calculated from the logarithm of the pressure levels by a linear interpolation (from here is the name PLOG):

$$\ln k = \ln k_j + \frac{\ln P - \ln P_j}{\ln P_{j+1} - \ln P_j} \cdot (\ln k_{j+1} - \ln k_j). \quad (23)$$

There are some reactions in which the reactants and the products are the same for both reactions, but the reaction depends on temperature in two different ways. These reactions can be described with two Arrhenius sets and are known as duplicated reactions.

## 2.2 The physical model: Radial bubble dynamics

The equation system to be resolved consists of ordinary differential equations (ODEs). The first equation is the modified Keller—Miksis equation [5] that describes the radial oscillation of a spherical bubble:

$$\left(1 - \frac{\dot{R}}{c_L}\right) \cdot R \cdot \ddot{R} + \left(1 - \frac{\dot{R}}{c_L}\right) \cdot \frac{3}{2} \cdot \dot{R}^2 = \left(1 + \frac{\dot{R}}{c_L} + \frac{R}{c_L} \cdot \frac{d}{dt}\right) \cdot \frac{(p_L(R, t) - p_{\infty}(t))}{\rho_L}. \quad (24)$$

Here,  $R$  is the bubble radius,  $t$  is the time,  $c_L$  is the liquid sound speed, and  $\rho_L$  is the liquid density. The connection between the pressure inside and outside the bubble is given by

$$p = p_L + \frac{2 \cdot \sigma}{R} + 4 \cdot \mu_L \cdot \frac{\dot{R}}{R}, \quad (25)$$

where  $\rho_L$  is the liquid pressure at the bubble wall,  $\sigma$  is the surface tension, and  $\mu_L$  is the dynamic viscosity of the liquid. The far-field pressure ( $p_{\infty}$ ) is constant (free oscillation):

$$p_{\infty}(t) = P_{\infty}, \quad (26)$$

where  $P_{\infty}$  is the ambient pressure. The internal pressure is calculated from the ideal gas law for the gas mixture:

$$p = M \cdot R_g \cdot T, \quad (27)$$

where  $M = \sum_{k=1}^K c_k$  is the total concentration of the mixture,  $R_g$  is the universal gas constant, and  $T$  is the internal temperature.

The temperature can be calculated via the first law of thermodynamics, written as

$$\dot{T} = \frac{-p \cdot \dot{V} - \sum_{k=1}^K (H_k \cdot \dot{\omega}_k) + \sum_{k=1}^K \dot{\omega}_k \cdot R_g \cdot T + \frac{\dot{Q}_{th}}{V}}{M \cdot \bar{C}_v}, \quad (28)$$

where  $V = 4 \cdot R^3 \cdot \pi/3$  is the volume of the bubble,  $\dot{Q}_{th}$  is the heat transfer at the bubble interface, and  $\bar{C}_v$  is the average molar heat capacity of the gas mixture in the bubble at constant volume. The molar heat capacity at constant pressure  $C_{p,k}$ , the molar enthalpy of formation  $H_k$  and the molar entropy  $S_k$  of the chemical species are described by the NASA polynomials as

$$\frac{C_{p,k}}{R_g} = \sum_{n=1}^N a_{n,k} \cdot T^{n-1}, \quad (29)$$

$$\frac{H_k}{R_g \cdot T} = \sum_{n=1}^N \frac{a_{n,k} \cdot T^{n-1}}{n} + \frac{a_{N+1,k}}{T}, \quad (30)$$

and

$$\frac{S_k}{R_g} = a_{1,k} \cdot \ln(T) + \sum_{n=1}^N \frac{a_{n,k} \cdot T^{n-1}}{n-1} + a_{N+2,k}, \quad (31)$$

where  $N = 5$  and  $a_{n,k}$  are the NASA coefficients. There are two sets of coefficients for the intervals  $[T_{low}, T_{mid}]$  and  $[T_{mid}, T_{high}]$ . The connection between the molar heat capacities are

$$C_{v,k} = C_{p,k} - R_g. \quad (32)$$

Some average values of the gas mixture need to be calculated. The mole fraction of component  $k$  ( $X_k$ ) is

$$X_k = \frac{c_k}{M}. \quad (33)$$

The average molar weight  $\bar{W}$ , the average molar heat capacity in constant pressure  $\bar{C}_p$  and in constant volume  $\bar{C}_v$ , and the average density  $\bar{\rho}$  are given by as follows:

$$\bar{W} = \sum_{k=1}^K X_k \cdot W_k, \quad (34)$$

$$\bar{C}_p = X_k \cdot C_{p,k}, \quad (35)$$

$$\bar{C}_v = X_k \cdot C_{v,k}, \quad (36)$$

and

$$\bar{\rho} = \sum_{k=1}^K c_k \cdot W_k. \quad (37)$$

Here  $W$  is the molecular weight, and the bars mean averaged values for the mixture.

For the heat transfer between the fluid and the bubble interior, the Toegel model is used [24]. In this model, there is a thin thermal boundary layer in which the temperature changes linearly from the bubble mean temperature  $T$  to the ambient liquid temperature  $T_0$ . The amount of heat transfer is approximated as

$$\dot{Q}_{th} = A \cdot \bar{\lambda} \cdot \frac{\partial T}{\partial r} \approx A \cdot \bar{\lambda} \cdot \frac{T_0 - T}{l_{th}}, \quad (38)$$

where  $A$  is the area of the bubble surface,  $\bar{\lambda}$  is the average thermal conductivity of the gas mixture, and  $l_{th}$  is the thickness of the thermal boundary layer, which is approximated as

$$l_{th} = \min \left( \sqrt{\frac{R \cdot \bar{\chi}}{\dot{R}}}, \frac{R}{\pi} \right), \quad (39)$$

where  $\bar{\chi}$  is the averaged thermal diffusivity of the mixture:

$$\bar{\chi} = \frac{\bar{\lambda} \cdot \bar{W}}{\bar{\rho} \cdot \bar{C}_p}. \quad (40)$$

The reaction enthalpies are taken into consideration in the changing of the internal energy, which is why the heat transfer is composed only of heat conduction:

$$\sum \dot{Q} = \dot{Q}_{th}. \quad (41)$$

The parameters and material properties of the physical model are summarized in Table 1. We assume that the bubble is placed in water, and its constant material properties are calculated at ambient temperature  $T_\infty$  (also given in Table 1). Since the ambient pressure  $P_\infty$  is a control parameter, see Section 3, its value is not specified.

**Table 1** Parameters and material properties of the numerical simulations

parameter	notation	value	units
liquid sound speed	$c_L$	1483	m/s
liquid density	$\rho_L$	998.2	kg/m <sup>3</sup>
surface tension	$\sigma$	0.07197	N/m
dynamic viscosity	$\mu_L$	0.001	Pa · s
ambient pressure	$P_\infty$		Pa
ambient temperature	$T_\infty$	293.15	K
universal gas constant	$R_g$	8.31446	J/(mol · K)

### 2.3 Structure of the governing equations

The governing equations are a set of ordinary differential equations (ODEs), which have the following structure. The Keller—Miksis equation describes the radial pulsation of the bubble and provides the evolution of the bubble radius  $R$  and bubble wall velocity  $\dot{R}$  as a function of time. This equation accounts for the inertia of the liquid domain and is responsible for the proper modeling of the compression mechanism of the gas content.

Via the first law of thermodynamics, the temperature  $T$  inside the bubble can be calculated. It takes into account the work done by the compression, the reaction enthalpies, and the heat transfer across the bubble interface.

With the help of the reaction mechanism described in Section 2.1, the following set of ODEs can be obtained for the concentrations of the chemical species inside the bubble:

$$\dot{c}_k = \dot{\omega}_k - c_k \cdot \frac{\dot{V}}{V}. \quad (42)$$

Assuming that the bubble initially contains only nitrogen and hydrogen and that the evaporation of the water is negligible (oxygen is excluded), only reactions involving elements N and H are necessary. This means altogether 36 chemical reactions and  $K = 14$  chemical species. The file of the mechanism in the Supporting Information originally contained all the reactions for the complete N-H-O system; therefore, the reactions involving the element O are commented out.

Altogether there are  $K + 3$  governing equations: two first-order systems from the Keller—Miksis equation (second-order ODE), a first-order system for the internal temperature, and  $K$  ODEs for the change of concentrations.

To close the equation system, the ideal gas law is employed for the gas mixture of the bubble content. This creates a relationship between volume, temperature, and pressure. Since the volume is calculated from  $R$  and the

temperature is obtained from the first law of thermodynamics, the ideal gas law is employed to calculate the internal pressure.

### 3 Control parameters and the numerical technique

The major parameters in a freely oscillating spherical bubble system are the equilibrium size of the bubble  $R_E$ ; the expansion ratio  $R_0/R_E$ , where  $R_0$  is the initial size of the bubble during the simulations (also the maximum bubble radius); the ambient pressure  $P_\infty$ ; and finally the initial composition of the bubble in terms of the percentage of hydrogen. Table 2 summarizes the employed values of the control parameters for a quick scan of the optimal parameter combination. The atmospheric pressure is denoted by  $p_{atm} = 101.3$  kPa. The total number of parameter combinations is  $7 \cdot 7 \cdot 13 \cdot 3 = 1911$ . Due to the stiff nature of the governing equations, only a small number of parameter combinations can be simulated within a reasonable time with the MATLAB built-in stiff solver (ode15s). It is shown in Section 5 that the optimum value often lies on one of the upper or lower limits of the specified parameters. In such cases, additional simulations are run to seek the optimum parameter combination.

The reason behind the parameter selection is as follows. The equilibrium bubble size describes how much is the amount of nitrogen and hydrogen gas inside the bubble. The larger the equilibrium size of the bubble, the more substance participates in the reactions. The expansion ratio describes the potential energy of the bubble; see Section 4 for more details. This is the energy that can be focused during the first collapse of the bubble and create extreme conditions. In the long term, all the potential energy is

**Table 2** Summary of the control parameters and their employed values

$R_0/R_E$ [-]	$R_E$ [ $\mu\text{m}$ ]	$P_\infty$ [Pa]	$P_\infty/p_{atm}$ [%]	% $\text{H}_2$ [%]
8.0	5.0	5066.25	5	65
9.0	7.5	10132.5	10	75
10.0	10.0	15198.75	15	85
11.0	12.5	20265	20	—
12.5	15.0	30397.5	30	—
15.0	20.0	40530	40	—
17.5	50.0	50662.5	50	—
—	—	60795	60	—
—	—	70927.5	70	—
—	—	81060	80	—
—	—	91192.5	90	—
—	—	101325	100	—
—	—	111457.5	110	—

dissipated by viscous forces. The ambient pressure is an important parameter from the input energy point of view. A large portion of the input energy is spent to displace the volume of the surrounding liquid. The lower the ambient pressure, the less energy is needed for such displacement. From stoichiometric considerations, the optimal initial composition of the bubble would be 75% hydrogen and 25% nitrogen. However, due to the triple bond of nitrogen and due to the short time scale of the extreme conditions, the internal composition of the bubble can be short of dissociated nitrogen. Thus, tuning the initial composition of the mixture might result in higher energy efficiency.

### 4 Energetic considerations of a freely oscillating bubble and the definition of the chemical yield

Fig. 1 shows a typical example of the dynamics and the chemical history of a freely oscillating bubble. In the upper panel, the bubble radius vs. time curve (blue) and the temporal evolution of the internal temperature (red) is depicted. The equilibrium bubble size is  $50 \mu\text{m}$ , which is expanded to  $400 \mu\text{m}$  representing an 8-fold expansion ratio. In the initial stage of the dynamics, the bubble starts to shrink since it is out of equilibrium. In later stages, due to the inertia of the surrounding liquid, the bubble radius swings through its equilibrium value, and a large compression ratio is realized with a peak temperature as high as about  $6000$  K. After the first collapse, the bubble loses most of its energy via shock wave (acoustic emission [25])

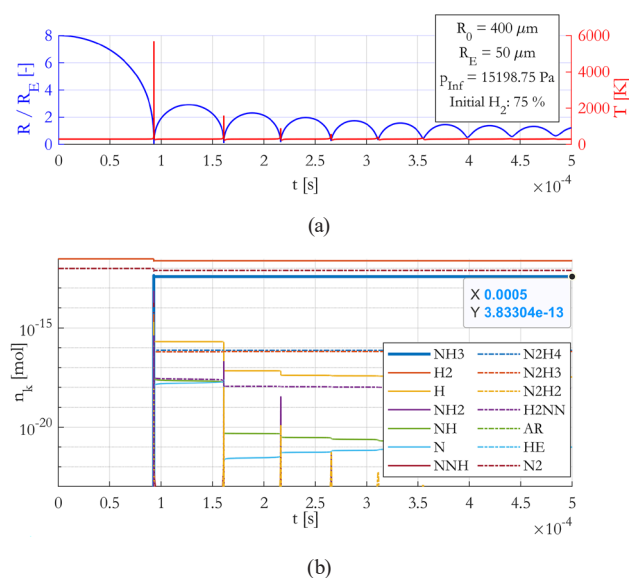


**Fig. 1** A typical example of the dynamics of a freely oscillating microbubble: (a) bubble radius and internal temperature as a function of time, (b) temporal evolution of the chemical species in moles (only nitrogen, hydrogen and ammonia are labelled)

indicated by the much smaller local maximum during the first rebound. In the subsequent dynamics, the oscillations are less rapid, the temperature peaks are less pronounced, and the long-term behavior of the bubble is the convergence to its equilibrium state.

The lower panel of Fig. 1 represents the temporal evolution of the chemical species inside the bubble in moles ( $n_k$ ). Initially, the bubble contains only nitrogen and hydrogen. Next, during the first collapse, around the minimum bubble radius, some of the nitrogen and hydrogen dissociates and other chemical species are produced. Observe that a large portion of the nitrogen (dashed-dot red curve) and hydrogen (solid red curve) do not dissociate; however, the main product of atomic N and H is ammonia (blue curve). The rest of the chemical species involved in the reaction mechanism have orders of magnitude lower concentration. The chemical yield of a bubble is defined as the amount of ammonia  $n_{\text{NH}_3}$  presented inside the bubble after chemical equilibrium is reached, which is the final time instant of the simulation denoted by the black dot in the lower panel on the blue curve.

The mass of the produced ammonia is calculated as

$$m_{\text{NH}_3} = n_{\text{NH}_3} \cdot M_{\text{NH}_3}, \quad (43)$$

where  $M_{\text{NH}_3}$  is the molar mass of the ammonia.

The potential energy

$$W_P = W_G + W_A + W_L \quad (44)$$

of the expanded bubble is composed of the work done by the internal gas during isothermal expansion (assuming that the expansion is slow)

$$W_G = -N_{i,0} \cdot R_g \cdot T_E \cdot \ln \left( \frac{R_{\text{max}}^3}{R_E^3} \right), \quad (45)$$

the work needed to enlarge the surface of the bubble against the surface tension

$$W_A = \sigma \cdot 4 \cdot \pi \cdot (R_{\text{max}}^2 - R_E^2), \quad (46)$$

and the work required to expand the bubble against the liquid domain

$$W_L = P_\infty \cdot \frac{4 \cdot \pi}{3} \cdot (R_{\text{max}}^3 - R_E^3); \quad (47)$$

that is the work needs to displace the volume of the liquid against the ambient pressure. The potential energy of the bubble can be considered as the required energy to expand the bubble from its equilibrium state  $R_E$  to its initial maximum size  $R_0$ .

It is important to take into account the energy to produce the hydrogen content. Assuming that the hydrogen is produced via electrolysis, the energy requirement of the hydrogen content can be calculated as

$$w_{\text{H}_2} = m_{\text{H}/\text{NH}_3} \frac{M_{\text{H}}}{M_{\text{NH}_3}} W_E, \quad (48)$$

where  $m_{\text{H}/\text{NH}_3}$  is the mass fraction of atomic hydrogen of ammonia molecule (its unit is t H/t  $\text{NH}_3$ ),  $M_{\text{H}}$  is the molar mass of hydrogen, and  $W_E = 180$  GJ/t H is the energy requirement of electrolysis of water.

The total input energy of the bubble system is composed of two components; namely, the energy required to expand the bubble and the energy to produce the hydrogen content (in units of GJ/t) is

$$w_{\text{TB}} = \frac{W_P}{m_{\text{NH}_3}} + w_{\text{H}_2}. \quad (49)$$

This value highly depends on the system parameters. The energy requirement of the Haber—Bosch process if the hydrogen is also produced via electrolysis is  $w_{\text{HB}} = 39.1$  GJ/t. During the parameter optimization, this is the baseline value with which the energy efficiency of the ammonia production by bubbles is compared.

### 5 Parameter optimization

In this section, the energy intensity as a function of the control parameters defined in Section 3 is explored based on the quantities introduced in Section 4.

Fig. 2 shows the energy intensity as a function of the equilibrium bubble size at different expansion ratios (color-coded curves). The ambient pressure and the initial

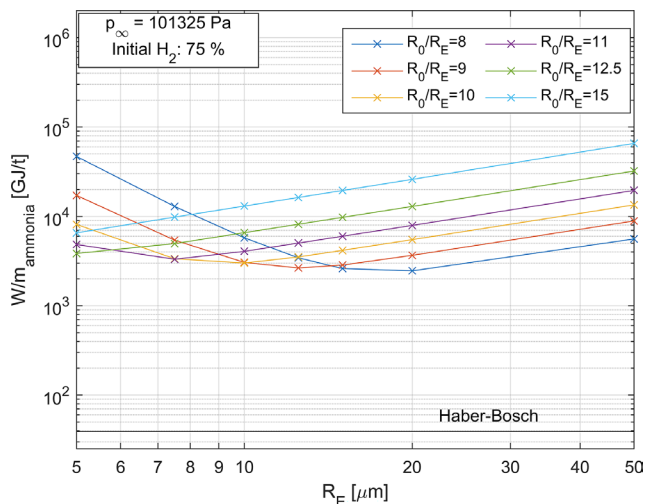


Fig. 2 Energy intensity of the ammonia production as a function of the equilibrium bubble size at different initial expansion ratios

composition of the bubble were atmospheric pressure ( $p_{atm} = 101.3 \text{ kPa}$ ) and the stoichiometric ratio of the hydrogen in ammonia (75% H), respectively. The energy intensity of the Haber—Bosch process is denoted by the horizontal black line. The optimum parameter combination is at  $R_E = 20 \text{ }\mu\text{m}$  and at  $R_0/R_E = 8$ . In this case, the energy intensity is 2455 GJ/t, which is approximately 62.8 times higher than the Haber—Bosch process.

In our experience, the major contribution of the potential energy is related to the liquid side via  $W_L$ . Therefore, reducing the ambient pressure can significantly decrease the required input energy to expand the bubble. Out of the 13 investigated ambient pressure values, Fig. 3 summarises the results of only two cases: 100% (dashed curves) and 5% (solid curves) of atmospheric pressure. Only three expansion ratios are depicted to avoid the overcrowding of Fig. 3. It is to be stressed that for simplicity, the energy required to produce a vacuum is not taken into account. This energy requirement is distributed amongst all the bubbles presented in a reactor. However, Eq. (49) is specified on a single bubble basis. Therefore, without the knowledge of the reactor design and the number density of the bubbles, the aforementioned energy requirement cannot be appropriately incorporated into Eq. (49).

By decreasing the ambient pressure, the energy intensity of the ammonia production drops significantly to 382 GJ/t, which is only 9.8 times higher than the Haber—Bosch process. However, the optimum bubble size is increased to the upper limit of the corresponding

parameter ranges, namely, to  $R_E = 50 \text{ }\mu\text{m}$ . Therefore, after examining the effect of the initial bubble composition, a broader range of equilibrium bubble sizes are examined at the end of this section.

Theoretically, the optimum initial composition of the bubble is 75% hydrogen and 25% nitrogen, assuming that all molecules dissociate and participate in the formation of ammonia. As is already depicted in Fig. 1, this is not the case, and a large portion of nitrogen and hydrogen molecules remain "intact". Since the energy to dissociate nitrogen is higher than that required for the hydrogen (due to the triple bond), it might seem feasible to shift the initial concentration towards nitrogen. For a 65% hydrogen content, the results are presented in Fig. 4 (solid curves). The ambient pressure is kept the same as in the case of the optimal one shown in Fig. 3. The corresponding results for the 75% hydrogen content are also represented by the dashed curves in Fig. 4. Albeit marginally, the energy intensity is further decreased to 351 GJ/t.

The final step of the optimization procedure is to examine the effect of the equilibrium bubble size on a wider range, see Fig. 5. The expansion ratio was a secondary parameter, while the ambient pressure and the initial hydrogen concentration were kept constant: 5066.25 Pa and 65%, respectively. The optimum equilibrium bubble size is increased to 165  $\mu\text{m}$ , and the optimum expansion ratio is decreased to  $R_0/R_E = 6$ . The energy intensity is decreased to 265.1 GJ/t. Therefore, compared to the Haber—Bosch process, this means a 6.78-fold difference.

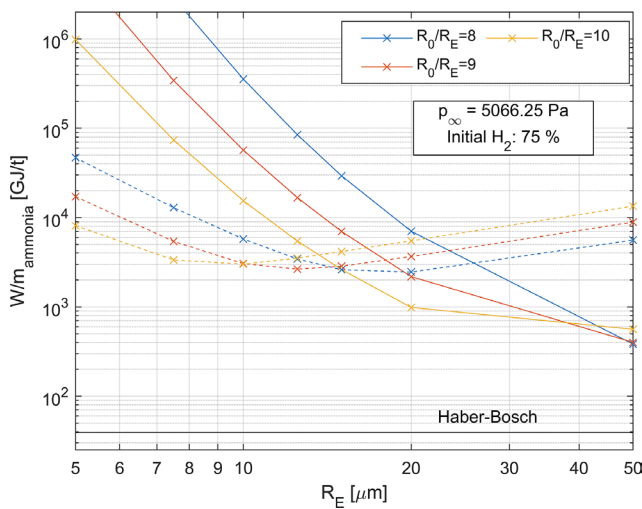


**Fig. 3** The effect of the ambient pressure on the energy intensity of the ammonia production. Dashed curves represent the results for atmospheric pressure; see Fig. 2. The solid line corresponds to a significantly lower ambient pressure value.

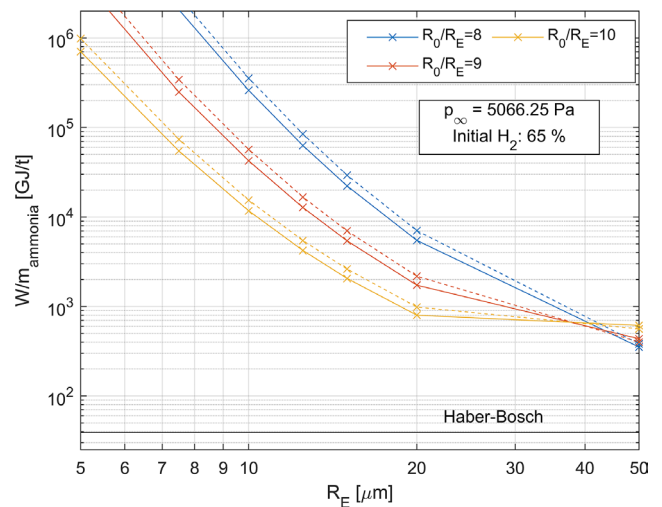


**Fig. 4** Effect of the variation of the initial composition of the microbubble. Dashed curves are solutions taken from Fig. 3. Solid curves represent energy intensities at a reduced hydrogen content.



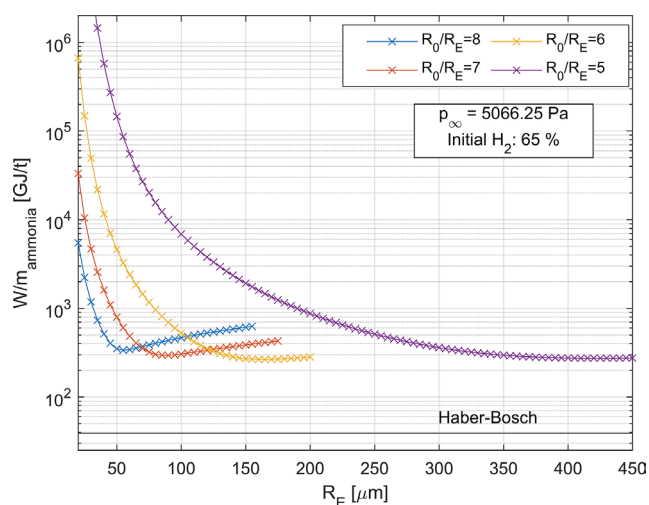


Fig. 5 Optimum bubble size to minimize energy intensity

## 6 Discussion and summary

The main aim of the present study was to investigate the theoretical energy efficiency of ammonia production via a freely oscillating bubble initially containing nitrogen and hydrogen. The input work is computed as the potential energy of the initially expanded bubble and the energy required to produce hydrogen by the electrolysis of water. The chemical yield is obtained via numerical simulations of the chemical history of the bubble. The control parameters were the equilibrium size of the bubble, initial expansion ratio, ambient pressure, and initial hydrogen concentration. At the best parameter combination, the energy intensity of ammonia production was 265.1 GJ/t. In comparison, the energy requirement of the Haber—Bosch process is 39.1 GJ/t (BAT with water electrolysis) or 46.2 GJ/t (global average).

Although the energy intensity of the ammonia production by bubbles is approximately 6.78 times higher than the BAT Haber—Bosch process, it is still several orders

of magnitude better than the available data in the literature [19]: 882353 GJ/t. Such a huge difference needs a theoretical explanation. In the experimental study of [19], the bubbles are generated via bubbling air throughout a vessel, and the bubble collapses are achieved by a 900 kHz ultrasonic irradiation. In some of our previous publications [7, 14], where the chemical computations are carried out for ultrasound excited bubbles, it turned out that significant chemical activity takes place only in the first few acoustic cycles. Afterwards, a dynamic equilibrium of the bubble content is settled. That is, the concentrations are continuously changing in time; however, their averaged values remain the same. In this regard, sonicating the same bubble for several minutes (millions of acoustic cycles) has a very little effect on the chemical yield, while continuously dissipating the input energy [26–28]. Therefore, the present theoretical work showed that ammonia production via microbubbles can still be a viable option; however, the operation strategy of such systems must be reconsidered.

## Acknowledgement

The research reported in this paper is part of project no. BME-NVA-02, implemented with the support provided by the Ministry of Innovation and Technology of Hungary from the National Research, Development and Innovation Fund, financed under the TKP2021 funding scheme. This paper was also supported by the János Bolyai Research Scholarship of the Hungarian Academy of Sciences and by the ÚNKP-22-2-I-BME-67 New National Excellence Program of the Ministry for Culture and Innovation from the source of the National Research, Development and Innovation Fund. The authors acknowledge the financial support of the Hungarian National Research, Development and Innovation Office via NKFIH grant OTKA FK142376.

## References

- [1] International Energy Agency (IEA) "Ammonia Technology Roadmap: Executive Summary", IEA, Paris, France, 2021. [online] Available at: <https://www.iea.org/reports/ammonia-technology-roadmap/executive-summary> [Accessed: 29 June 2023]
- [2] Appl, M. "Ammonia: Principles and industrial practice", Wiley–VCH, 1999. ISBN 9783527295937  
<https://doi.org/10.1002/9783527613885>
- [3] Rafiqul, I., Weber, C., Lehmann, B., Voss, A. "Energy efficiency improvements in ammonia production—perspectives and uncertainties", *Energy*, 30(13), pp. 2487–2504, 2005.  
<https://doi.org/10.1016/j.energy.2004.12.004>
- [4] Valera-Medina, A., Xiao, H., Owen-Jones, M., David, W. I. F., Bowen, P. J. "Ammonia for power", *Progress in Energy and Combustion Science* 69, pp. 63–102, 2018.  
<https://doi.org/10.1016/j.peccs.2018.07.001>
- [5] Lauterborn, W., Kurz, T. "Physics of bubble oscillations", *Reports on Progress in Physics*, 73, 106501, 2010.  
<https://doi.org/10.1088/0034-4885/73/10/106501>
- [6] Leighton, T. G. "The Acoustic Bubble", Academic Press, 2012. ISBN 978-0124124981
- [7] Kalmár, C., Klapcsik, K., Hegedűs, F. "Relationship between the radial dynamics and the chemical production of a harmonically driven spherical bubble", *Ultrasonics Sonochemistry*, 64, 104989, 2020.  
<https://doi.org/10.1016/j.ultsonch.2020.104989>
- [8] Yasui, K., Tuziuti, T., Kozuka, T., Towata, A., Iida, Y. "Relationship between the bubble temperature and main oxidant created inside an air bubble under ultrasound", *The Journal of Chemical Physics*, 127(15), 154502, 2007.  
<https://doi.org/10.1063/1.2790420>

- [9] Stricker, L., Lohse, D. "Radical production inside an acoustically driven microbubble", *Ultrasonics Sonochemistry*, 21(1), pp. 336–345, 2014.  
<https://doi.org/10.1016/j.ultsonch.2013.07.004>
- [10] Kerboua, K., Hamdaoui, O. "Influence of reaction heats on variation of radius, temperature, pressure and chemical species amounts within a single acoustic cavitation bubble", *Ultrasonics Sonochemistry*, 41, pp. 449–457, 2018.  
<https://doi.org/10.1016/j.ultsonch.2017.10.001>
- [11] Yasui, K., Kato, K. "Bubble dynamics and sonoluminescence from helium or xenon in mercury and water", *Physical Review Letters*, 86, 036320, 2012.  
<https://doi.org/10.1103/PhysRevLett.86.036320>
- [12] Kerboua, K., Hamdaoui, O. "Numerical investigation of the effect of dual frequency sonication on stable bubble dynamics", *Ultrasonics Sonochemistry*, 49, pp. 325–332, 2018.  
<https://doi.org/10.1016/j.ultsonch.2018.08.025>
- [13] Rashwan, S. S., Dincer, I., Mohany, A. "A unique study on the effect of dissolved gases and bubble temperatures on the ultrasonic hydrogen (*sonohydrogen*) production", *International Journal of Hydrogen Energy*, 45(41), pp. 20808–20819, 2020.  
<https://doi.org/10.1016/j.ijhydene.2020.05.022>
- [14] Kalmár, C., Turányi, T., Zsély, I. G., Papp, M., Hegedűs, F. "The importance of chemical mechanisms in sonochemical modelling", *Ultrasonics Sonochemistry*, 83, 105925, 2022.  
<https://doi.org/10.1016/j.ultsonch.2022.105925>
- [15] Yasui, K., Kato, K. "Numerical simulations of sonochemical production and oriented aggregation of BaTiO<sub>3</sub> nanocrystals", *Ultrasonics Sonochemistry*, 35, pp. 673–680, 2017.  
<https://doi.org/10.1016/j.ultsonch.2016.05.009>
- [16] Brennen, C. E. "Cavitation and Bubble Dynamics", Oxford University Press, 1995. ISBN 0-19-509409-3
- [17] Mettin, R. "From a single bubble to bubble structures in acoustic cavitation", In: Kurz, T., Parlitz, U., Kaatz, U. (eds.) *Oscillations, Waves and Interactions*, Universitätsverlag Göttingen, 2007, pp. 171–198. ISBN 978-3-938616-96-3
- [18] Mettin, R. "Bubble structures in acoustic cavitation", In: Doinikov, A. A. (ed.) *Bubble and Particle Dynamics in Acoustic Fields: Modern Trends and Applications*, Research Signpost, 2005, pp. 1–36. ISBN 9788177362848
- [19] Supeno, Kruus, P. "Fixation of nitrogen with cavitation", *Ultrasonics Sonochemistry*, 9(1), pp. 53–59, 2002.  
[https://doi.org/10.1016/S1350-4177\(01\)00070-0](https://doi.org/10.1016/S1350-4177(01)00070-0)
- [20] Klapcsik, K. "GPU accelerated numerical investigation of the spherical stability of an acoustic cavitation bubble excited by dual-frequency", *Ultrasonics Sonochemistry*, 77, 105684, 2021.  
<https://doi.org/10.1016/j.ultsonch.2021.105684>
- [21] Klapcsik, K. "Dataset of exponential growth rate values corresponding non-spherical bubble oscillations under dual-frequency acoustic irradiation", *Data in Brief*, 40, 107810, 2022.  
<https://doi.org/10.1016/j.dib.2022.107810>
- [22] Haghi, H., Sojahrood, A. J., Kolios, M. C. "Collective nonlinear behavior of interacting polydisperse microbubble clusters", *Ultrasonics Sonochemistry*, 58, 104708, 2019.  
<https://doi.org/10.1016/j.ultsonch.2019.104708>
- [23] Otomo, J., Koshi, M., Mitsumori, T., Iwasaki, H., Yamada, K. "Chemical kinetic modeling of ammonia oxidation with improved reaction mechanism for ammonia/air and ammonia/hydrogen/air combustion", *International Journal of Hydrogen Energy*, 43(5), pp. 3004–3014, 2018.  
<https://doi.org/10.1016/j.ijhydene.2017.12.066>
- [24] Toegel, R., Gompf, B., Pecha, R., Lohse, D. "Does water vapor prevent upscaling sonoluminescence?", *Physical Review Letters*, 85(15), 3165, 2000.  
<https://doi.org/10.1103/PhysRevLett.85.3165>
- [25] Sojahrood, A. J., Haghi, H., Karshafian, R., Kolios, M. C. "Nonlinear model of acoustical attenuation and speed of sound in a bubbly medium", In: 2015 IEEE International Ultrasonics Symposium (IUS), Taipei, Taiwan, 2015, pp. 1–4. ISBN 978-1-4799-8182-3  
<https://doi.org/10.1109/ULTSYM.2015.0086>
- [26] Louisnard, O. "Nonlinear attenuation of sound waves by inertial cavitation bubbles", *Physics Procedia*, 3(1), pp. 735–742, 2010.  
<https://doi.org/10.1016/j.phpro.2010.01.093>
- [27] Jamshidi, R., Brenner, G. "Dissipation of ultrasonic wave propagation in bubbly liquids considering the effect of compressibility to the first order of acoustical Mach number", *Ultrasonics*, 53(4), pp. 842–848, 2013.  
<https://doi.org/10.1016/j.ultras.2012.12.004>
- [28] Hegedűs, F., Kalmár, C., Turányi, T., Zsély, I. G., Papp, M. "Chapter 4 - Sonochemical reactions, when, where and how: Modelling approach", In: Hamdaoui, O., Kerboua, K. (eds.) *Energy Aspects of Acoustic Cavitation and Sonochemistry*, Elsevier, 2022, pp. 49–77. ISBN 978-0-323-91937-1  
<https://doi.org/10.1016/B978-0-323-91937-1.00013-X>